Design of Silicon Nitride Edge Coupler for Monolithically Integrated Laser on Silicon Photonic Circuits With Relaxed Alignment Tolerance and High Efficiency

Yisu Yang, Kaixiang Gao, Huiyuan Zhang, Huaibing Liu, Xinyuan Lu, Xiaomin Ren, *Senior Member, IEEE*, and Yongqing Huang, *Member, IEEE*

***Abstract*—We propose a bi-layer 5-tip edge coupler in a multi-layer silicon nitride-on-silicon (SiN-on-Si) waveguide platform. The coupler is used for the integration between a monolithic 1550 nm laser and a single-mode SiN waveguide. The simulated coupling efficiency is 92.8%. The vertical 1-dB-loss misalignment tolerance is as large as 0.5 μm. Broad 1-dB-drop bandwidth (1338 nm to 1700 nm) and small footprint (total length: 38.2 μm) are achieved simultaneously. A broadband bi-layer SiN-Si adiabatic transition cascaded to the edge coupler is designed to couple the laser power into a single-mode Si waveguide at an efficiency of 90.6%. Low-computation-cost electromagnetic numerical simulation and optimization strategies are applied to improve the reverse design of the complex couplers.**

***Index Terms*—Integrated nanophotonic systems, silicon nanophotonics, theory and design, waveguides.**

I. Introduction

SILICON (Si) photonics offers a powerful platform attempting to leverage the maturity of Si complementary metal oxide semiconductor (CMOS) processing techniques to apply it to the domain of optoelectronics [1], [2]. The monolithic laser can provide high-density integrated light sources for Si photonics with lithography-controlled in-plane alignment [3], [4]. However, the efficient coupling between the laser and a standard Si waveguide on a silicon-on-insulator (SOI) wafer still presents challenges due to poor mode matching and a refractive index difference between the light source and passive waveguides. Two standard approaches in Si photonics platforms to couple to on-chip waveguides are with surface grating couplers (GCs) and edge couplers (ECs) [5], [6]. The EC is usually an inverse taper that can expand the spatial distribution of the mode profile outside the waveguide core via shrinking the tip width to match the incident mode. ECs are preferred over GCs in applications where a broad optical bandwidth or polarization-insensitive coupling or in-plane packaging are needed. This makes ECs a better candidate in laser-to-chip coupling especially for edge-emitting monolithic laser integration. This kind of laser is featured by high-power and long lifetime [3], [4]. Complex ECs for fiber-to-chip coupling have been developed to reduce coupling loss and to improve alignment tolerance. Spot-size converters, incorporating lower-index waveguides or tapers, are overlaid on Si waveguides for the mode field diameter (MFD) expansion in ECs [5]–[7]. To our knowledge, this method has so far not been fully investigated for laser-to-chip monolithic coupling. Recent publications demonstrated the integration of a laser die through a Si EC and the reported insertion loss was around 2 dB [8]–[10].

However, there are two issues related to the EC coupling scheme. Firstly, the vertical misalignment tolerance of the conventional Si EC that has one waveguiding layer is still small (<500 nm) for the pick-and-place tools for high-volume production. Secondly, the monolithically integrated laser usually has thick (about 3 μm) buffer layers to block the defects from threading dislocation. This makes the coupling between the laser and a standard Si EC difficult because the Si photonics devices fabricated by CMOS foundries usually use a 220-nm-thick Si waveguiding layer on top of the 2-μm-thick buried oxide (BOX) layer. Even if the monolithic laser is grown from the top of the Si substrate of the SOI wafer, the laser emission position is still much higher than the Si EC waveguide plane. In this case, the laser-to-chip in-plane coupling is impossible due to incompatible structures. In the face of these two challenges, we would like to seek help from new photonic materials and multilayer photonic integration platforms. For instance, silicon

Manuscript received February 17, 2022; revised March 12, 2022; accepted March 16, 2022. Date of publication March 18, 2022; date of current version April 7, 2022. This work was supported in part by the Research Innovation Fund for College Students of Beijing University of Posts and Telecommunications, in part by the National Natural Science Foundation of China under Grant 61904016, in part by the National Key Research and Development Program of China under Grant 2018YFB2200104, and in part by the Beijing Municipal Science and Technology Commission under Grant Z191100004819012. *(Corresponding author: Yisu Yang.)*

Yisu Yang, Xiaomin Ren, and Yongqing Huang are with the State Key Laboratory of Information Photonics and Optical Communications, Alferov Russian-Chinese Joint Lab of Information Optoelectronics & Nanoheterostructures, and BUPT-Hengtong Joint Lab of Quantum Optoelectronics & Bivergentum Theory, Beijing University of Posts and Telecommunications, Beijing 100876, China (e-mail: yangyisu916@163.com; xmren@bupt.edu.cn; yqhuang@bupt.edu.cn).

Kaixiang Gao, Huiyuan Zhang, Huaibing Liu, and Xinyuan Lu are with the School of Electronic Engineering, Beijing University of Posts and Telecommunications, Beijing 100876, China (e-mail: gaokaixiangdach@163.com; zhanghuiyuan@bupt.edu.cn; 2309708871@bupt.edu.cn; 18736220253@163.com).

Digital Object Identifier 10.1109/JPHOT.2022.3160669

nitride (SiN) is a CMOS-compatible material. It is low-loss over a broad operation range from visible (~400 nm) to the mid-infrared wavelength (~4 μm), expanding the Si-based photonic integrated circuits (PICs) to various applications [11], [12]. In recent years, both the academic and industry communities have shown great interest in Si photonics with three-dimensional (3-D) SiN photonic integration platforms and SiN-based on-chip lasers [13], [14].

In this work, we design a bi-layer 5-tip SiN EC for the monolithic Si laser integration. We propose a multilayer SiN-on-SOI waveguide platform to couple between the vertical levels of the laser emission and Si waveguiding layer and use an automatic optimization method to design an EC that has well-balanced performance. In our design, a monolithic laser is efficiently butt-coupled to a single-mode SiN channel waveguide by this EC. Simulations show that high coupling efficiency (92.8%), good vertical misalignment tolerance, broad 1-dB-drop bandwidth (362 nm across the optical communication band), and small footprint (38.2 μm in length) can be obtained simultaneously.

II. Theory and Design Method

A bi-layer 5-tip SiN EC is the key component for the laser-to-chip integration in our design. We choose the structure because of the trade-off between the fabrication capability and the coupling performance. If more than two SiN layers are fabricated, foundry processes cannot deposit high-quality thick SiN waveguiding layers by PECVD. If we use the single-layer edge coupler, there will be a small mode area along the vertical direction. Besides, a single SiN layer makes the vertical alignment between the monolithic laser emission port and the center of EC challenging as we will discuss later. So the bi-layer is a promising choice in the view of fabrication and mode overlap. If more than five tips are used, the improvement of coupling efficiency is neglectable, but the fabrication uncertainty will increase rapidly. If fewer tips are used, the mode area will not be expanded enough to match our laser mode profile along the horizontal direction. The 5-tip pattern was automatically optimized by a large-scale screening. It took a short time to find the optimum results since the simulation was based on the finite difference method (FDM) with a low computational cost [15]. We propose a multilayer SiN-on-SOI photonic integration platform to build the EC as illustrated in Fig. 1(a, b). The platform consists of two 400-nm-thick Si_3N_4 layers and a 220-nm-thick Si layer separated by SiO_2 spacers. The BOX layer thickness is 2 μm. The separation between the lower and upper Si_3N_4 layers (referred to as SiN1 and SiN2 respectively) is 330 nm in height, and the separation between the Si and SiN1 layers is 250 nm. The thicknesses of the BOX layer and the Si layer are chosen to match that of the Si photonics foundry process [1]. The thicknesses of other SiN and SiO_2 layers are optimized to realize a large overlap between the EC mode and the laser mode in our design. To solve the alignment issues between the different stacks of the laser and the EC, we chose to use multiple thick SiN and SiO_2 layers compatible with the foundry CMOS processes. The object is to align the laser emission position with the EC center, which is about 3.1 μm above the Si substrate.

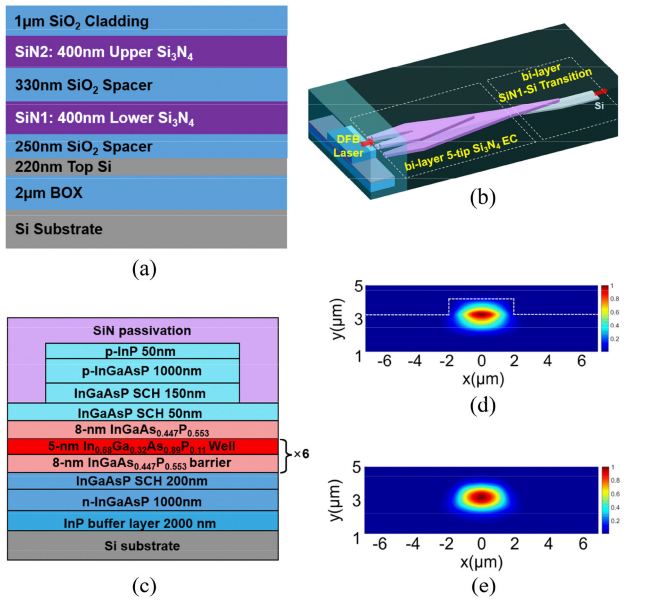

Fig. 1. (a) Schematic of the SiN-on-SOI waveguide platform with the thicknesses labeled; (b) 3-D illustration of a bi-layer 5-tip SiN EC butt-coupled with an III-V DFB laser on Si; (c) heteroepitaxial structure of the surface ridge III-V laser on Si. SCH: separate confinement heterostructure; (d) the fundamental TE mode profile of the laser; (e) the lasing field pattern after passing through the 1-μm-wide SiN coupling trench. Normalized $|E_x|^2$ is shown in (d, e) and the top of the Si substrate is at y = 0.

The refractive indices were taken to be 3.48, 1.44, and 1.96 for the Si, SiO_2, and SiN, respectively. The optical power from a monolithic laser can be efficiently coupled into a single-mode SiN1 waveguide by the SiN EC. A 1-μm-wide coupling trench is present between the facet of the III-V laser and the EC. The trench is filled with SiN anti-reflection coating to improve laser performance. This platform supports previously reported bi-layer SiN1-Si adiabatic transition [11]. This transition can be cascaded after the EC to transfer the coupled light into the Si waveguiding layer. This enables access to active Si photonics devices such as Si modulators and germanium photodetectors [16], [17].

Firstly, we designed a 1550 nm monolithic III-V ridge Distributed-FeedBack (DFB) laser and characterized the special laser mode that was different from the fiber mode. This is the critical condition for the SiN EC design. The III-V epitaxy layers were grown on the Si substrate of our SiN-on-SOI waveguide platform with a 2-μm-thick InP buffer layer as shown in Fig. 1(c). The stack definition was similar to the lasers previously fabricated [4], [18]. To align with the EC in the vertical direction (y-axis) as shown in Fig. 1(b), we trimmed the thickness of the bottom InGaAsP cladding layer to 1 μm and the center of the lasing mode was about 3.1 μm above the Si substrate as shown in Fig. 1(d). For better lasing mode confinement and laser-to-chip mode coupling, we optimized the ridge width of the laser to 4 μm. We numerically calculated the fundamental transverse electric (TE) lasing mode by the FDM. After passing the coupling trench, lasing light arrived at the input interface of the EC. At that interface, we simulated the lasing pattern (E_1) while not the EC fundamental mode (E_2) by the finite-difference

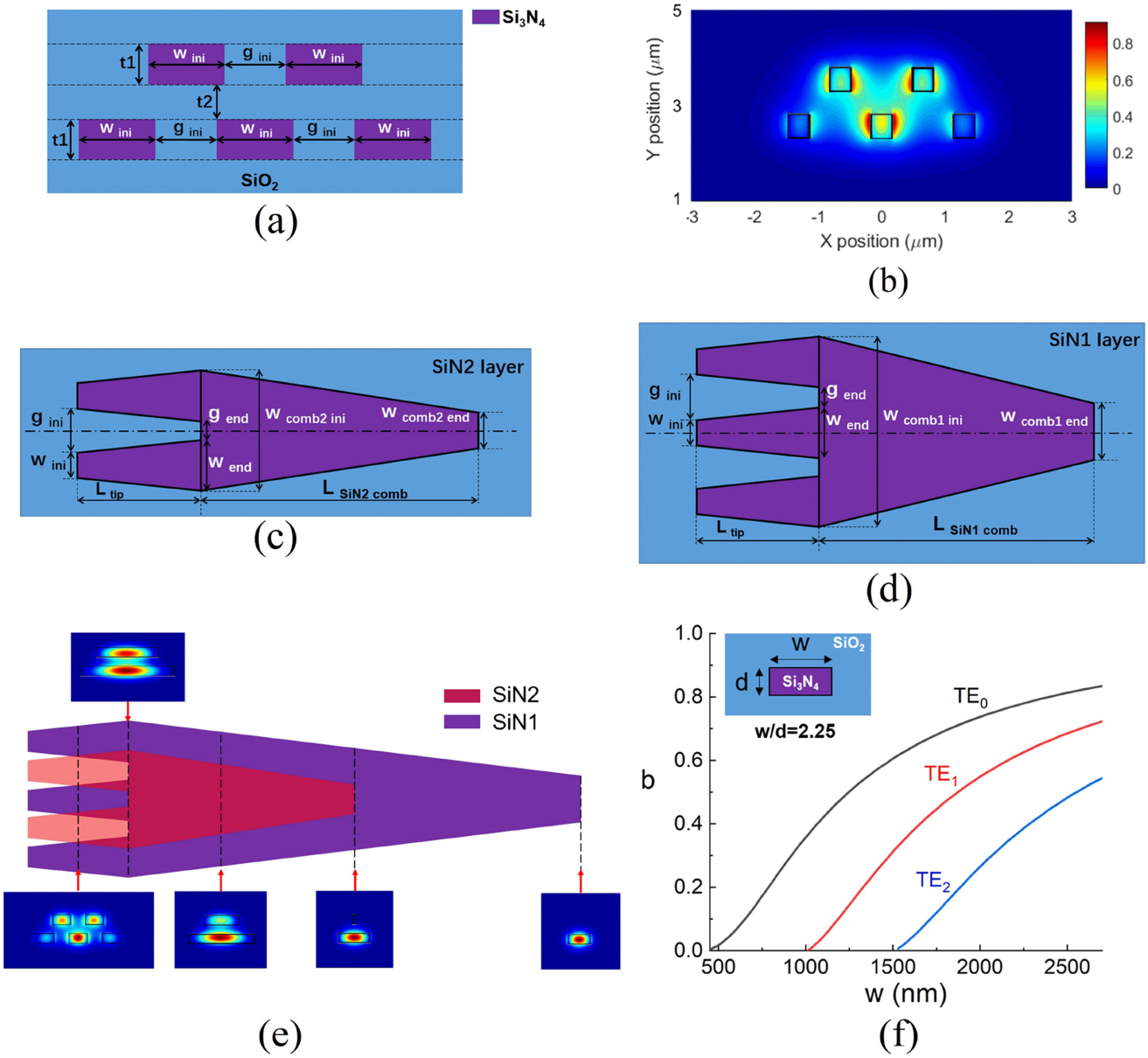

Fig. 2. (a) Cross-sectional view of the bi-layer 5-tip SiN EC at the input interface; (b) mode intensity profile ($|E_x|^2$) of the fundamental TE mode (TE_0) of the EC at the input interface; (c, d): top view of the EC in the SiN2 and SiN1 layers; (e) top-down schematics of the EC and mode intensity profiles are shown at multiple points along with the EC; (f) dispersion curves of the SiN channel waveguide (inset: a cross-sectional view of the waveguide); normalized propagation constant $b = (n_{eff}^2 - n_0^2)/(n_1^2 - n_0^2)$; n_{eff} : mode effective index; n_0: SiO_2 refractive index; n_1: SiN refractive index. Modes are calculated at a wavelength of 1550 nm.

time-domain (FDTD) method, using an open-source software package [19]. The laser MFDs are 3.3 μm along the x-axis and 2.0 μm along the y-axis as shown in Fig. 1(e). The ellipse-like lasing pattern is different from the circular fiber mode that has been well studied in a traditional EC. In the following steps, we just need to import the lasing pattern without performing the FDTD-based simulations between the laser and the EC input interface again to reduce the computational cost.

The total coupling efficiency (η_c) of the bi-layer 5-tip SiN EC is determined by the input interface coupling efficiency (η_i) between the lasing field pattern as shown in Fig. 1(e) and the mode of EC at the input interface as shown in Fig. 2(a, b). The η_c is also influenced by the mode evolution efficiency (η_m) that is determined by how well the mode evolves adiabatically from the EC input interface to the single-mode SiN1 waveguide. And η_c can be expressed as $\eta_c = \eta_i \cdot \eta_m$. The bi-layer 5-tip EC consists of a multi-tip section (L_{tip}), an upper SiN2 combiner section ($L_{SiN2\ comb}$), and a lower SiN1 combiner section ($L_{SiN1\ comb}$) as shown in Figs. 1(b) and 2(a, c-e). The complex geometry of the EC offers design flexibility to achieve better coupling compared with the conventional inverse taper EC. However, the optimization is challenging due to a large number of design parameters. Besides, we have multiple design objects including high η_c, broad optical bandwidth ($\Delta\lambda$), large misalignment tolerance, and small footprint. To satisfy the design goals, we applied

the Multiple-Object-DIvided-RECTangular (MODIRECT) algorithm to automatically search for the practical values of w_{ini}, g_{ini}, w_{end}, L_{tip}, $L_{SiN1\ comb}$, and $L_{SiN2\ comb}$. Compared with the conventional particle swarm optimization, MODIRECT is a global optimization method and is less likely to have the problem of premature convergence [20], [21].

We carried out the optimization of the EC based on the reverse design principles [22] as follows: (i) the FDM was used to find the mode field of the EC. Then, (ii), η_i was determined by the mode overlap integral [23] as shown in Eq. (1) at the EC input interface. The reflection at the two sides of the input interface was also considered. And, (iii), the FDTD method was used to calculate the η_m. Lastly, (iv), the total coupling efficiency, η_c, was calculated and was used as the fitness value for the MODIRECT to iterate through steps (i) to (iii) to obtain the optimized design parameters.

We found that the difference of simulated η_i was less than 2% between the FDM and the FDTD. The later numerical method is generally believed to have higher accuracy. Thus, good simulation accuracy of the FDM was verified. Moreover, the FDM had a much lower computational cost compared with the FDTD. We performed extensive FDM simulations to optimize the layer stack thicknesses as shown in Fig. 1(a) in order to obtain the maximum η_i. After the EC, we design an adiabatic linear tapered bi-layer SiN1-Si transition to transfer optical power from the SiN1 layer to the Si layer as shown in Fig. 1(b). The input and output of the transition are single-mode waveguides with widths of 500 nm in the 220-nm-thick Si layer and 900 nm in the 400-nm-thick SiN1 layer. To reduce the power consumption, the single-mode waveguides that have low loss are desired. The shape of the transition is also optimized by the MODIRECT.

$$\eta = \frac{\left(\int\int_{-\infty}^{\infty} E_1(x,y)E_2^*(x,y)dxdy\right)^2}{\int\int_{-\infty}^{\infty} E_1(x,y)E_1^*(x,y)dxdy \int\int_{-\infty}^{\infty} E_2(x,y)E_2^*(x,y)dxdy}. \quad (1)$$

III. Simulation Results and Discussion

We fixed the stack thicknesses of the monolithic III-V DFB laser and SiN-on-SOI waveguide platform based on the vertical alignment requirements. In the bi-layer 5-tip EC design, the optimization of η_i took 3.3 hours after 292 times of iteration as shown in Fig. 3(a). During this time, we optimized the w_{ini} and g_{ini} by MODIRECT and found the coupler mode only by the FDM. Then, we optimized the values of L_{tip}, $L_{SiN1\ comb}$, $L_{SiN2\ comb}$, w_{end}, and $w_{combin2\ end}$ by MODIRECT and simulated the field propagation by the FDTD method. This took about 26 hours. As for other parameters, $w_{combin1\ ini}$ and $w_{combin2\ ini}$ were determined by g_{end} and w_{end}; g_{end} was equal to the feature size of the lithography to reduce the mode mismatch between the multi-tip section and the combiner section; $w_{combin1\ end}$ was 900 nm to build a single-mode SiN1 output waveguide. By the EC, the mode evolved smoothly and gradually from the mode size of the laser to the mode size in the 900 nm × 400 nm SiN1 channel waveguide as shown in Fig. 2(e). After finding the optimum parameters, the simulations were repeated five times for the whole EC using different fine FDTD mesh grids (mesh size: 5 nm to 20 nm). The results were consistent. When the tapered tips in the two SiN layers became wider in the multi-tip section, the peak intensity of the mode gradually moved to the outer edge of the tip, and more power was confined in the gap between adjacent tips. We attribute this to the low index contrast of the SiN waveguide. This could speed up the mode evolution and contribute to the short multi-tip section with high coupling efficiency. We calculated the normalized propagation constant (b) [24] of the channel waveguide as a function of the waveguide width (w) and thickness (d) in order to find the geometry of the single-mode waveguide. We selected $w/d = 2.25$ in order to put our designed parameters ($w = 900$ nm, $d = 400$ nm) in the dispersion curve. And the designed SiN channel waveguide can support single-mode (TE_0) operation as shown in Fig. 2(f). We performed all the simulations on a personal computer with a 3.2 GHz CPU and an 8 GB physical RAM. The SiN EC geometry parameters are summarized in Table I.

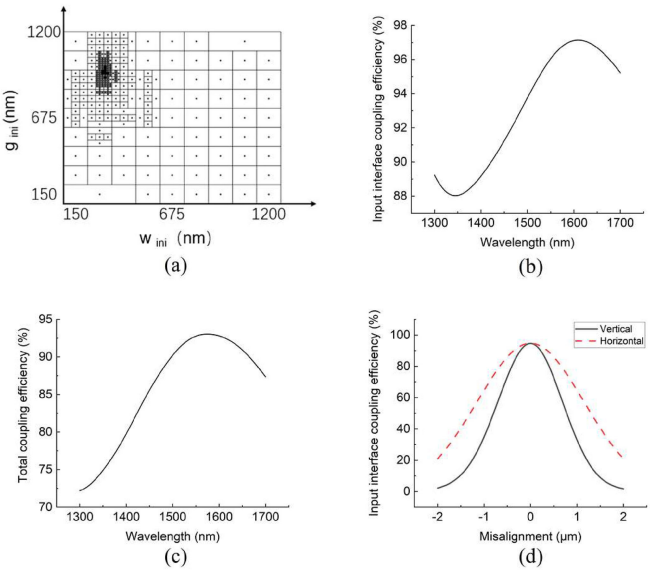

Fig. 3. Simulation results of the EC: (a) the convergence of w_{ini} and g_{ini} after 292 iterations by MODIRECT; (b) input interface coupling efficiency (η_i) as a function of wavelengths; (c) total coupling efficiency (η_c) as a function of wavelengths; (d) η_i as a function of the misalignment of the light source.

TABLE I
Optimized Parameters of the Bi-Layer 5-tip SiN EC

Parameters	Size(nm)	Parameters	Size(nm)
w_{ini}	351	$w_{comb1\ ini}$	3759
w_{end}	1153	$w_{comb2\ ini}$	2456
g_{ini}	952	$w_{comb1\ end}$	900
g_{end}	150	$w_{comb2\ end}$	200
L_{tip}	13235	$L_{SiN1\ comb}$	25000
$t1$	400	$L_{SiN2\ comb}$	20680
$t2$	330		

The η_i and η_c of the bi-layer 5-tip EC as functions of incident wavelength are shown in Fig. 3(b, c). At 1550 nm, the η_i of 97.6% and η_c of 92.8% were achieved. $\Delta\lambda$ was greater than 362 nm for η_c >74% (1338 nm-1700 nm). This estimation was limited by the available experimental data of the SiN

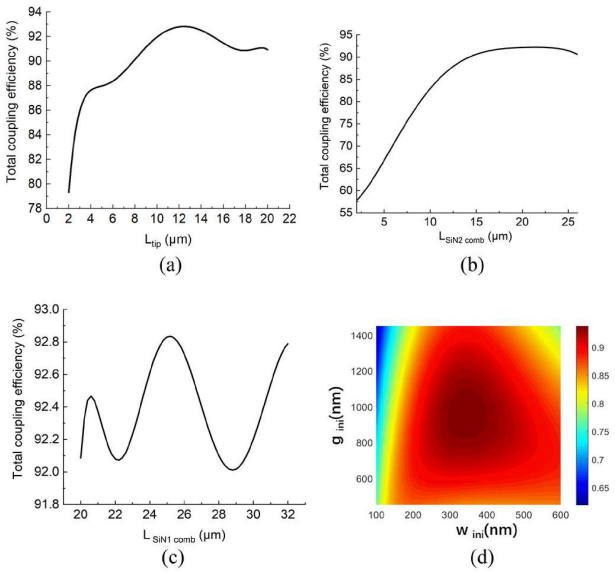

Fig. 4. Simulated η_c as a function of (a) multi-tip section length, (b) upper SiN2 combiner section length, (c) lower SiN1 combiner section length; (d) simulated η_i as a function of w_{ini} and g_{ini}. Simulation wavelength: 1550 nm. Other parameters are listed in Table I.

TABLE II
COMPARISON OF VARIOUS DESIGNS OF MULTI-TIP ECS ON SOI PLATFORM AT 1550 NM FOR LASER-TO-CHIP COUPLING

Structure (sim: simulation)	y/x-axis misalignment tolerance for 1dB loss penalty (μm)	Min feature size (nm)	Coupling efficiency	Total device length (μm)	1dB bandwidth (nm)	Laser integration method
5-tip [10]	0.5/1.9	180	48.9%	156.7	28	Hybrid FP
2-tip [9]	NA	100	58.9%	150	NA	Hybrid FP
4-tip [8] (sim)	0.41/0.77	150	90.7%	90	415	Hybrid DFB
5-tip this work (sim)	0.5/0.8	150	92.8%	38.2	362	Monolithic DFB

refractive index. By the FDM and mode overlap integral, we found that vertical and horizontal misalignment tolerances at 1550 nm for a 1-dB-loss penalty of η_i were 0.5 μm and 0.8 μm, respectively, as shown in Fig. 3(d). Further, η_i was greater than 50% if the vertical/horizontal misalignment was smaller than 0.8/1.3 μm. The misalignment tolerance is large enough for the monolithic laser integration. This coupler could also be used in hybrid laser integration since the tolerance is larger than the placement accuracy of $\pm$0.5 μm which can be achieved by using a commercial die bonder [25]. We attribute this improvement in coupling tolerance to the multilayer multi-tip EC that expands the mode area.

The influences of L_{tip}, $L_{SiN1\ comb}$, and $L_{SiN2\ comb}$ on η_c were shown in Fig. 4(a-c). The mapping in Fig. 4(d) shows how the η_i changes with the parameters g_{ini} and w_{ini} around their optimized values. This indicates that the EC has large tolerance of fabrication errors. The total length of the EC along the propagation direction is 38.2 μm (multi-tip section: L_{tip} = 13.2 μm; maximum length of the combiner sections: $L_{SiN1\ comb}$ = 25 μm). The small footprint is significant for the high-density 3-D photonic integration. Table II compares this work with other multi-tip EC demonstrations. The major difference between our work and others is that we design a

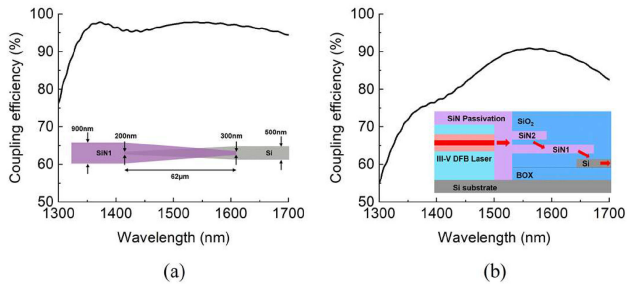

Fig. 5. Simulated results of the bi-layer SiN1-Si transition and the laser-to-Si coupling scheme: (a) coupling efficiency of the SiN1-Si transition for the TE polarization as a function of incident wavelengths. Inset: Top-down schematic of the transition; (b) coupling efficiency from the monolithic laser to a single-mode Si channel waveguide. Inset: cross-sectional view of the laser-to-waveguide coupling.

3-D photonic integration platform. Thus, we can build a bi-layer coupler to expand the mode area easily in both x- and y-direction. If only one 220-nm-thick Si layer is used [8]–[10], the mode area cannot be expanded effectively in the y-direction. The other difference is that we choose a specially designed monolithic laser. The mode profiles and layer thickness were both optimized in the laser and passive devices. The improvement of misalignment is shown by the absolute value of coupling efficiency although the values of y-axis misalignment tolerance for 1-dB loss penalty are the same in [10] and our work. We admit that the coupling efficiency of our EC will decrease to some extent in the real experiment due to the change of laser mode profile and the non-ideal laser-to-chip interface that may introduce back-reflection. The critical fabrication steps are polishing and dicing. They are applied to fabricate the coupling trench and interface of the EC. If these processes are reliable and accurate, the EC performance will be guaranteed.

Next to the EC, we designed a bi-layer SiN1-Si transition as shown in the inset of Fig. 5(a). The Si waveguide tapers down to a blunt tip with a 200-nm-width, and the SiN1 waveguide tapers to blunt tips of 300-nm-width. The taper length is 62 μm. We simulated the coupling efficiency from the single-mode SiN1 channel waveguide to the single-mode Si channel waveguide for the TE polarization by the FDTD method as shown in Fig. 5(a). The coupling efficiency is greater than 95% from the wavelength of 1342.7 nm to 1687.6 nm. The peak efficiency is 97.8% at 1537.7 nm and the efficiency is 97.6% at the lasing wavelength of 1550 nm. The coupling efficiency decreases at shorter wavelengths as the optical confinement in the Si and SiN increases. When the optical power propagates through the SiN EC and the SiN-Si transition, the total coupling efficiency from the laser emission facet to the single-mode Si channel waveguide is 90.6% at 1550 nm as shown in Fig. 5(b). The efficiency is greater than 90% from the wavelength of 1530.8 nm to 1607.7 nm. In the real experiment, the coupling efficiency is expected to be smaller due to waveguide propagation losses. The total waveguide length along the propagation direction including one bi-layer 5-tip EC and one bi-layer SiN1-Si transition is close to 100 μm as shown in Figs. 1(b) and 5(a), which may contribute an additional loss to the total propagation of 0.01-0.05 dB for average propagation losses of 1-5 dB/cm. Even considering

these negative influences, our SiN EC and SiN-Si transition still offer competitive solutions for the low-loss, broadband, and compact monolithic laser integration in both passive and active Si photonics chips.

IV. Conclusion

A bi-layer 5-tip edge coupler on a customized SiN-on-Si waveguide platform for direct coupling with a monolithically integrated III-V-on-Si laser was proposed. This platform can be tailored to match the vertical position of the laser emission, which is typically 1 μm higher than the Si waveguiding layer of a Si platform, with the edge coupler. Coupling from the laser output mode into a single-mode SiN waveguide with the edge coupler has high coupling efficiency ($\eta_c = 92.8\%$ @1550 nm) and broad 1-dB-drop bandwidth (1338 nm-1700 nm), taking only a small footprint (total coupling length: 38.2 μm). The coupler is misalignment tolerant (vertical/horizontal 1-dB-loss misalignment penalty: 0.5/0.8 μm). This edge coupler platform also supports a high-efficiency broadband bi-layer SiN1-Si adiabatic transition, enabling access to active Si-based building blocks such as Si modulators and Ge photodetectors. Practical reverse design strategies were developed, which can be used as a general approach for the design of laser-to-chip edge couplers tailorable to other material platforms.

Acknowledgment

Y. Yang thanks J. C. C. Mak and A. Novack for critically reading the manuscript and their feedback.

References

[1] S. Siew *et al.*, "Review of silicon photonics technology and platform development," *J. Lightw. Technol.*, vol. 39, no. 13, pp. 4374–4389, Jul. 2021, doi: 10.1109/JLT.2021.3066203.

[2] W. Bogaerts and L. Chrostowski, "Silicon photonics circuit design: Methods, tools and challenges," *Laser Photon. Rev.*, vol. 12, no. 4, Apr. 2018, Art. no. 1700237, doi: 10.1002/LPOR.201700237.

[3] J. Norman *et al.*, "A review of high performance quantum dot lasers on silicon," *IEEE J. Quantum Electron.*, vol. 55, no. 2, Apr. 2019, Art. no. 2000511, doi: 10.1109/JQE.2019.2901508.

[4] M. Tang *et al.*, "Integration of III-V lasers on Si for Si photonics," *Prog. Quantum Electron.*, vol. 66, pp. 1–18, Aug. 2019, doi: 10.1016/J.PQUANTELEC.2019.05.002.

[5] R. Marchetti, C. Lacava, L. Carroll, K. Gradkowski, and P. Minzioni, "Coupling strategies for silicon photonics integrated chips," *Photon. Res*, vol. 7, no. 2, pp. 201–239, Feb. 2019, doi: 10.1364/PRJ.7.000201.

[6] X. Mu, S. Wu, L. Cheng, and H. Fu, "Edge couplers in silicon photonic integrated circuits: A review," *Appl. Sci.*, vol. 10, no. 4, Feb. 2020, Art. no. 1538, doi: 10.3390/APP.10041538.

[7] Y. Lin *et al.*, "Low-loss broadband bi-layer edge couplers for visible light," *Opt. Exp.*, vol. 29, no. 21, pp. 34565–34576, Oct. 2021, doi: 10.1364/OE.435669.

[8] Y. Tu, P. Fu, and D. Huang, "High-efficiency ultra-broadband multi-tip edge couplers for integration of distributed feedback laser with silicon-on-insulator waveguide," *IEEE Photon. J.*, vol. 11, no. 4, Aug. 2019, Art. no. 6602113, doi: 10.1109/JPHOT.2019.2924477.

[9] N. Hatori *et al.*, "A hybrid integrated light source on a silicon platform using a trident spot-size converter," *J. Lightw. Technol.*, vol. 32, no. 7, pp. 1329–1336, Apr. 2014, doi: 10.1109/JLT.2014.2304305.

[10] S. Romero-Garcia, B. Marzban, F. Merget, B. Shen, and J. Witzens, "Edge couplers with relaxed alignment tolerance for pick-and-place hybrid integration of III-V lasers with SOI waveguides," *IEEE J. Sel. Top. Quantum Electron.*, vol. 20, no. 4, pp. 369–379, Jul./Aug. 2014, Art. no. 8200611, doi: 10.1109/JSTQE.2013.2292523.

[11] W. Sacher *et al.*, "Monolithically integrated multilayer silicon nitride-on-silicon waveguide platforms for 3-D photonic circuits and devices," *Proc. IEEE*, vol. 106, no. 12, pp. 2232–2245, Dec. 2018, doi: 10.1109/JPROC.2018.2860994.

[12] J. Liu *et al.*, "High-yield, wafer-scale fabrication of ultralow-loss, dispersion-engineered silicon nitride photonic circuits," *Nat. Commun.*, vol. 12, Apr. 2021, Art. no. 2236, doi: 10.1038/S41467-021-21973-z.

[13] C. Xiang *et al.*, "Narrow-linewidth III-V/Si/Si_3N_4 laser using multilayer heterogeneous integration," *Optica*, vol. 7, pp. 20–21, Jan. 2020, doi: 10.1364/OPTICA.384026.

[14] S. Kumari, E. Haglund, J. Gustavsson, A. Larsson, G. Roelkens, and R. Baets, "Vertical-cavity silicon-integrated laser with in-plane waveguide emission at 850 nm," *Laser Photon. Rev.*, vol. 12, no. 2, Feb. 2018, Art. no. 1700206, doi: 10.1002/LPOR.201700206.

[15] P. Lüsse, P. Stuwe, J. Schüle, and H. Unger, "Analysis of vectorial mode fields in optical waveguides by a new finite difference method," *J. Lightw. Technol.*, vol. 12, no. 3, pp. 487–494, Mar. 1994, doi: 10.1109/50.285331.

[16] J. Witzens, "High-speed silicon photonics modulators," *Proc. IEEE*, vol. 106, no. 12, pp. 2158–2182, Dec. 2018, doi: 10.1109/JPROC.2018.2877636.

[17] A. Novack *et al.*, "Germanium photodetector with 60 GHz bandwidth using inductive gain peaking," *Opt. Exp.*, vol. 21, no. 23, pp. 28387–28393, Nov. 2013, doi: 10.1364/OE.21.028387.

[18] K. Dridi, A. Benhsaien, J. Zhang, and T. Hall, "Narrow linewidth 1550 nm corrugated ridge waveguide DFB lasers," *IEEE Photon. Technol. Lett.*, vol. 26, no. 12, pp. 1192–1195, Jun. 2014, doi: 10.1109/LPT.2014.2318593.

[19] A. Oskooi, D. Roundy, M. Ibanescu, P. Bermel, J. Joannopoulos, and S. Johnson, "MEEP: A flexible free-software package for electromagnetic simulations by the FDTD method," *Comput. Phys. Commun.*, vol. 181, no. 3, pp. 687–702, Mar. 2010, doi: 10.1016/J.CPC.2009.11.008.

[20] J. Mak, Q. Wilmart, S. Olivier, S. Menezo, and J. Poon, "Silicon nitride-on-silicon bi-layer grating couplers designed by a global optimization method," *Opt. Exp.*, vol. 26, no. 10, pp. 13656–13665, May 2018, doi: 10.1364/OE.26.013656.

[21] A. Al-Dujaili and S. Suresh, "Dividing rectangles attack multi-objective optimization," in *Proc. IEEE Congr. Evol. Computation*, Vancouver, Canada, Jul. 2016, pp. 3606–3613.

[22] L. Su, D. Vercruysse, J. Skarda, N. Sapra, J. Petykiewicz, and J. Vučković, "Nanophotonic inverse design with SPINS: Software architecture and practical considerations," *Appl. Phys. Rev.*, vol. 7, no. 1, Mar. 2020, Art. no. 011407, doi: 10.1063/1.5131263.

[23] A. Yariv and P. Yeh, "Optical resonators," in *Photonics: Optical Electronics in Modern Communications*, 6th ed., New York, NY, USA: Oxford Univ., 2007, pp. 204–206.

[24] K. Okamoto, "Planar optical waveguides," in *Fundamentals of Optical Waveguides*. San Diego, CA, USA: Academic, 2000, pp. 18–22.

[25] H. Moos, "Optical package assembly," Mar. 2022. [Online]. Available: https://www.finetechusa.com/knowledge/technical-papers-bonding/optical-packages-assembly/